MICROSTRUCTURE EVOLUTION AND MICROMECHANISMS OF SUPERPLASTICITY IN A HIGH STRENGTH Al-Zn-Mg-Cu ALLOY

John Liu and Dhruba J. Chakrabarti
Aluminum Company of America, Alcoa Technical Center, 100 Technical Drive
Alcoa Center, PA15069, U.S.A.

Abstract

The overall microstructure and texture changes corresponding to the different regions of the stress-strain curve during superplastic forming (SPF) can be understood by considering the three types of deformation mechanisms involved: dislocation slip, grain boundary sliding (GBS) and grain rotation. Grain structure and microtexture evolution during SPF were studied on a high strength, unrecrystallized Al-Zn-Mg-Cu superplastic alloy sheet using the SEM-based local orientation technique covering a large number of (sub)grain boundaries. Samples were deformed to different strains at 477°C and $\dot{\varepsilon}=0.002s^{-1}$. The results of our work suggest that in response to the applied stress, dislocation slip was operative initially, and continued to be important until the stress maximum was approached. Detailed misorientation analysis clearly identified that GBS initiated at a small strain corresponding to the very early portion of the stress-strain curve before the stress maximum, and was expected to continue throughout the entire SPF process. Grain rotation was steadily operative from the outset, as indicated by the steady increase in the misorientation of the low angle subgrains, but it did not contribute to any major microstructural changes before the stress maximum. No abrupt microstructural change occurred at the stress maximum, discounting the earlier speculation of dynamic recrystallization. Quantitative ODF analysis of local texture data indicated that grain rotation, which resulted in texture randomization, became important from slightly beyond the stress maximum through most of the stress-strain curve. Interestingly, a weak Goss texture, a known discontinuous recrystallization texture component, appeared at later stages of SPF.

Introduction

An important class of SPF aluminum alloys is characterized by an initial unrecrystallized structure stable at the elevated test temperatures, e.g., Supral [1], Al-Mg-X [2] and several other aluminum alloys, including the current 7050 base composition with Sc additions [3]. During the SPF, this structure evolves into one with fine grains without involving nucleation and growth associated with the classical (discontinuous) recrystallization. The term "continuous recrystallization" has been used to describe it. The precise micromechanisms to account for the stress assisted high temperature relaxation of these alloys at various stages of the SPF process is still unclear, although grain boundary sliding (GBS) and grain rotation have been identified as being important [2, 4].

A complete and statistically meaningful mechanistic study to follow the evolution of microstructure during superplastic straining requires a local study of microstructure at the subgrain level as well as a study of a large number of contiguous (sub)grains. In the current

work, the limitation of spatial coverage associated with the TEM approach [2,4] was overcome by the SEM-based backscattered Kikuchi diffraction technique [5]. The objective of the current study was to provide important experimental evidence which sheds light on how, at elevated temperatures and under stress, an equiaxed structure with predominantly high angle boundaries can evolve from a low angle subgrain structure.

Experimental

The starting material was a 2.54 mm thick high strength Al-Zn-Mg-Cu alloy SPF sheet produced from Alcoa's patented composition and process [3], giving 695% elongation to failure at a strain rate ($\dot{\varepsilon}$) of 0.002 s^{-1}. The gage length of the specimen was 9.375 mm, and the tests were performed at 447°C under a constant strain rate. For the current studies, samples were pulled to true strains of 0.1, 0.2, 0.4, 0.75 and 1.30, respectively. Samples were rapidly quenched in cold water from the test temperature for microstructure study. A ~5 mm thick section of the SPF sample was mounted on a plane normal to the transverse direction, metallographically polished, anodized, and viewed under polarized light to study the evolution of grain structure with strain. The sample was then prepared for misorientation and microtexture analysis in the SEM by the backscattered Kikuchi Diffraction technique. Higher resolution microstructure imaging was accomplished by SEM channeling contrast.

The orientation measurements were made at mid-thickness along both the rolling direction (RD) and the normal direction (ND) near the mid-gage location. Some measurements also were made at the grip for the condition of no strain. For each strain, about 100 measurements were made along the RD distributed over 10 separate elongated bands of grains, and about 50 measurements along the ND distributed likewise over 5 bands. For $\varepsilon = 0.75$, additional measurements along the RD were made at distances of 2.5, 5.0 and 7.5 mm from the mid-gage for intermediate strains.

Results

The starting as-deformed sheet comprised a heavily banded unrecrystallized structure under the optical microscope. Upon thermal exposure to 477°C, only a few scattered elongated recrystallized grains formed in the grip region of the test specimen where there was no strain. In contrast, the gage microstructure, controlled by the concurrent effects of test temperature and deformation, showed systematic evolution with strain. At the strains of 0.1 and 0.2, the gage microstructure was not noticeably different from that of the grip, Figure 1. At the $\varepsilon = 0.4$ corresponding to the load maximum, the diffused boundaries within the banded structure began to sharpen, and additional elongated, recrystallized grains were observed. At $\varepsilon = 0.75$, the banded structure was substantially replaced by a more equiaxed and uniform grain structure. At $\varepsilon = 1.3$, the optical microstructure resembled an equiaxed "recrystallized" structure, Figure 1. In addition:

1. The microstructure at $\varepsilon = 0.4$ was far from being fully recrystallized.
2. The elongated recrystallized grains that formed either statically or during straining were completely replaced in subsequent stages by smaller equiaxed grains.

SEM channeling contrast showed that the equiaxed (sub)grain size increased with increasing strain from about 2.3 μm at $\varepsilon = 0$ to about 6.8 μm at $\varepsilon = 1.3$, Figure 2. Importantly, no abnormal localized grain growth was observed.

Misorientation angles between contiguous grains and subgrains along both the RD and the ND, and the corresponding misorientation distribution histograms are presented in Figures 3 through 5. The results for $\varepsilon = 0$ were similar to those for the $\varepsilon = 0.1$ condition, and only those for the latter will be discussed. The misorientation traces show that along the RD a number of contiguous low angle subgrains were aligned along its length between adjacent high angle boundaries, Figure 3(a). In contrast, along the ND, the bands usually contained one or two low

angle subgrains, Figure 3(c). In both the directions, the high angle boundaries were primarily derived from the as-cast grains. In the misorientation traces shown, data from each array of measurements were plotted next to each other for convenience.

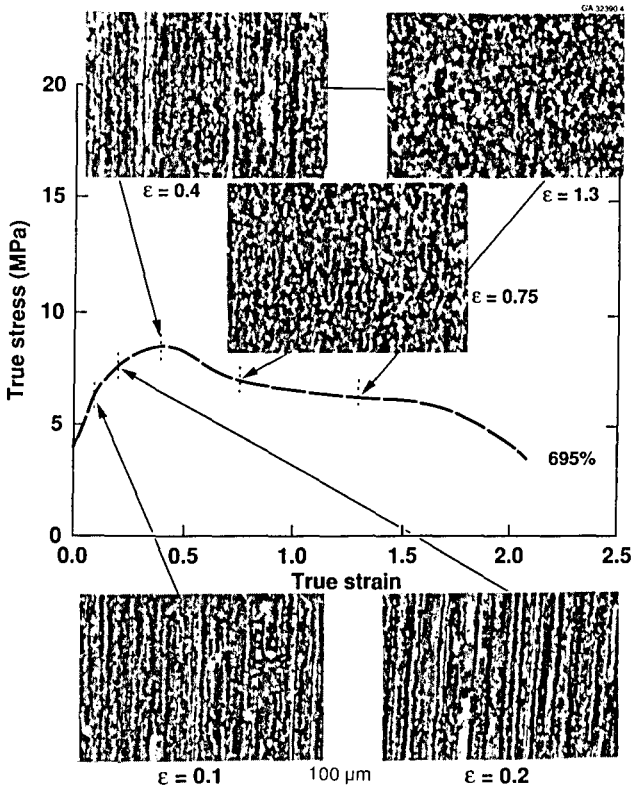

Figure 1. Optical micrographs showing microstructure evolution with strain during superplastic tensile testing.

The misorientation data for each sample were grouped arbitrarily into seven different bins in increments of 9°, with the largest range of 54° to 63°, covering close to the theoretical maximum of 62.8°. Misorientation was considered "low" for angles less than 18°. The population at each misorientation interval for $\varepsilon = 0.1$ is shown in Figure 3(b) for the RD and in Figure 3(d) for the ND. Along the RD, about 90% of the boundaries were low angle type. In contrast, along the ND the misorientation spread throughout the entire range. At $\varepsilon = 0.2$, neither the misorientation distribution nor the local texture changed noticeably. At $\varepsilon = 0.4$ along the RD, the population of low angle boundaries <9° was clearly reduced and that from 9° to 18° increased slightly, although there was a net total reduction of low angle boundaries, Figures 4(a, b). A concurrent increase in population occurred in the 36° to 63° misorientation range. However, no significant increase in population was observed at the intermediate 18° to 36°misorientation range. Thus, the transition from the low misorientation to the high misorientation (>36°) appeared to occur abruptly.

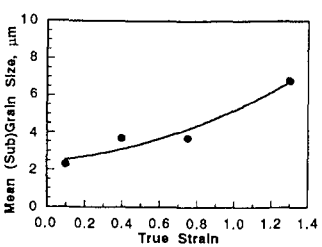

Figure 2. Effect of strain on mean (sub)grain size.

At $\varepsilon = 0.75$ along the RD, the lower bound of the misorientation angle was noticeably raised, and the array of low angle boundaries was interrupted more frequently by medium and high angle boundaries, Figure 4(c). The population of low angle boundaries dropped dramatically, and the population at all higher angle groups was correspondingly increased, Figure 4(d). The transition of misorientation distribution from $\varepsilon = 0.4$ to $\varepsilon = 0.75$ was very large. Therefore, the sample was examined at three

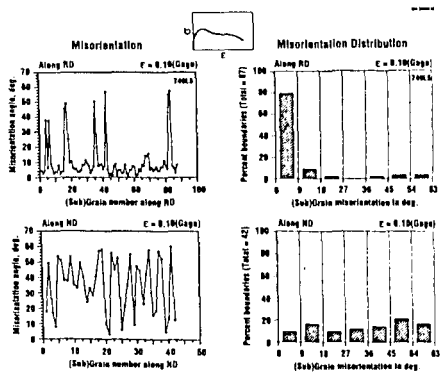

(a) (b)
(c) (d)

Figure 3. Misorientation traces (a, c) and misorientation distributions (b, d) in gage section along RD and ND after SPF test to $\varepsilon = 0.1$.

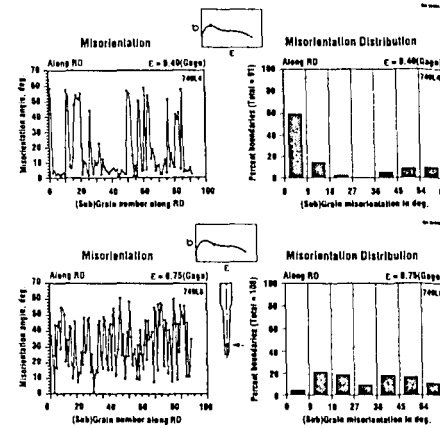

(a) (b)
(c) (d)

Figure 4. Misorientation traces (a, c) and misorientation distributions (b, d) in gage section along RD after SPF test to $\varepsilon = 0.4$ (a, b) and $\varepsilon = 0.75$ (c, d).

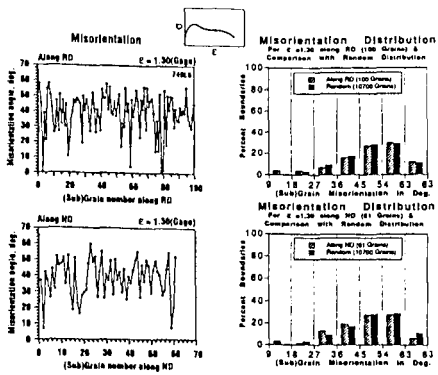

(a) (b)
(c) (d)

Figure 5. Misorientation traces (a, c) and misorientation distributions (b, d) in gage section along RD and ND after SPF test to $\varepsilon = 1.3$; comparison with random distribution in (b) and (d).

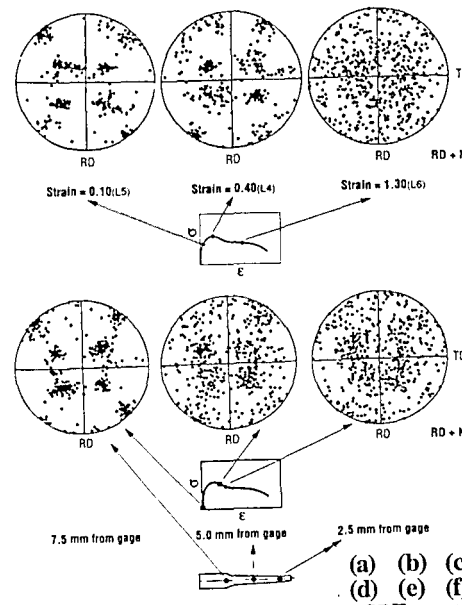

(a) (b) (c)
(d) (e) (f)

Figure 6. (200) pole figures after SPF test to $\varepsilon = 0.1$ (a), $\varepsilon = 0.4$ (b), $\varepsilon = 0.75$ (c) and for $\varepsilon = 0.75$ at locations 7.5mm (d), 5.0mm (e) and 2.5mm (f) from mid-gage.

additional locations, namely 2.5, 5.0 and 7.5 mm away from the mid-gage, to represent the three gradually decreasing strain levels. As anticipated, the low angle population along the RD was incrementally higher, but no population surge still occurred at the medium misorientation range.

At $\varepsilon = 1.3$, the misorientation traces and the misorientation distribution each looked similar along both the RD and ND, and each compared very closely to a simulated random distribution [6], Figures 5(a) through 5(d). The appearance of randomness was consistent with the disappearance of the banded grains, and their replacement by nearly equiaxed grains in the optical micrographs, Figure 1 and in the SEM image.

Combined RD and ND micro-texture is presented in the form of (200) micro-pole figures in Figures 6(a), 6(b), 6(f) and 6(c) for samples with strains, 0.1, 0.4, 0.75 and 1.30, respectively. For the $\varepsilon = 0.1$, a strong {110}<112> "brass" texture, which is the characteristic rolling texture for aluminum alloys, was observed, Figure 6(a). The strong brass texture persisted at $\varepsilon = 0.4$, Figure 6(b). Along with the increase in the highly misoriented boundaries, a randomization of the local texture appeared to occur at $\varepsilon = 0.75$, Figure 6(f), which resembled that for $\varepsilon = 1.3$, Figure 6(c). In order to study the apparently rapid texture transition between $\varepsilon = 0.4$ and $\varepsilon = 0.75$, the latter sample was studied at the same three locations to bridge the texture transition as before. The results showed that the transition from the brass to a random texture with strain was not abrupt, but was gradual and progressive, Figures 6(d) through 6(f).

Discussion

In general, microstructural changes up to $\varepsilon = 0.4$ were subtle. The optical studies for the $\varepsilon = 0.4$ condition indicated that the stress maximum was not associated with any abrupt microstructural change, Figure 1, contrary to the earlier belief of the completion of dynamic recrystallization at that strain [1]. From the SEM channeling contrast microstructure, the (sub)grain size determined as a function of strain, Figure 2, also showed no abrupt change in the rate of (sub)grain growth. Further, the microtexture results, Figure 6(b), showed that a very strong brass deformation texture remained at the stress maximum. These observations ruled out the occurrence of dynamic recrystallization at this point.

The misorientation studies provided insight into the nature of the grain structure beyond morphological changes. The grain structure comprised largely low angle subgrains at low strains, and predominantly high angle grains at large strains. Also, the initial texture consisting of essentially the {110}<112> brass component was replaced by a very diffused, nearly random texture at large strains. Referring to the pole figure for $\varepsilon = 0.1$, Figure 6(a), two orientations of the same brass variant must result in a low angle subgrain boundary. Conversely, the pole figure corresponding to $\varepsilon = 1.3$ lacks any clustering appearance, and is not likely to have been made up of low angle subgrains, Figure 6(c). Hence, the local pole figures supported the results of the above misorientation studies.

Having described the overall changes in grain morphology, misorientation and microtexture with SPF strain, a more detailed analysis of the current results was performed by classifying the misorientation angles into low angle and high angle types. For numerical convenience, the misorientation angles for all the (sub)grains measured were classified as low angle if the value was less than 18°, and as high angle above 18°. The mean misorientation angle for the low angle subgrains is plotted as a function of strain in Figure 7(a), and the fraction of high angle grains versus strain in Figure 7(b). To determine if any other micromechanisms were operative, the local textures obtained for each strain condition were further studied by the Orientation Distribution Functions (ODF's) for a more quantitative analysis and for the detection of any weak texture components. Each of the individual orientations was superimposed with a Gaussian peak of 5° spread. Then the spherical harmonic method was applied to obtain the continuous ODF [7]. This analysis, in general agreement with the pole figure results, showed that the initial texture consisted of essentially only the {110}<112> brass component with a

peak intensity of 32 times random, Figure 8. As shown, the φ_2=0° section alone contained essentially all the important texture information. Figures 9(a) through (g) show the φ_2=0° ODF sections for all the strain levels studied.

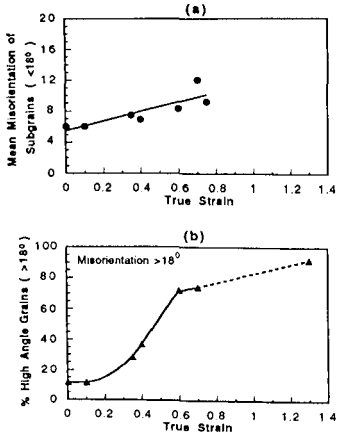

Figure 7. Effect of strain on (a) mean misorientation of subgrains (< 18°), and (b) percentage of high angle grains (>18°).

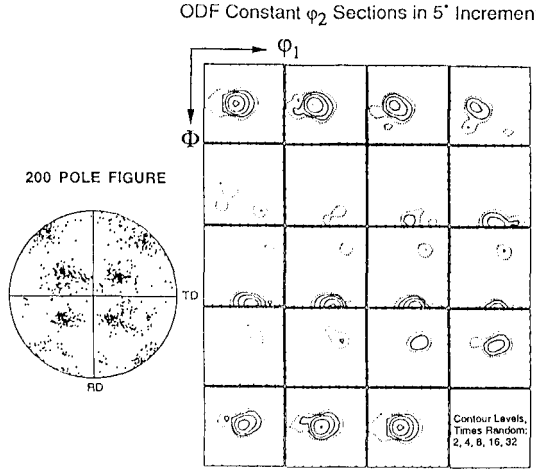

Figure 8. (200) pole figure and corresponding ODF plots for thermal exposure alone (no strain).

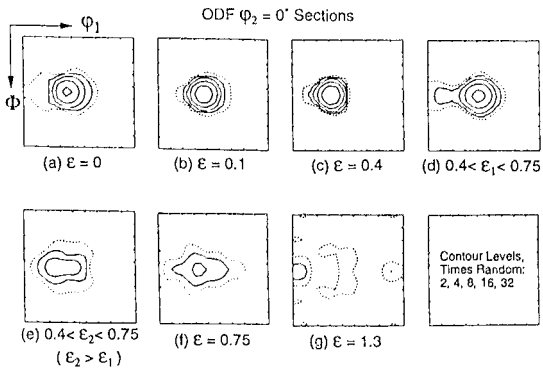

Figure 9. φ_2=0° ODF sections for increasing strain conditions.

The shape of the stress-strain curve along with the above misorientation and microtexture analyses provide important information on the underlying deformation mechanisms: dislocation slip, GBS and grain rotation. Diffusional accommodation, while operative, does not directly impact the major focus of this study, and will not be treated here. Dislocation slip in response to the applied stress is associated with work hardening, and contributes to the positive slope on the stress-strain curve. To a first approximation, GBS based on the Ashby/Verrall model [8] involving grain switching is not expected to result in significant texture randomization. The important aspect of GBS is that each GBS event involving low angle boundaries is expected to result in the abrupt development of high angle boundaries due to the switching of grain neighbors. Grain rotation, on the other hand, should give rise to a progressive increase in misorientation with a concurrent randomization of the initial deformation texture.

With the above simple physical models in mind, the underlying operative micromechanisms

during SPF corresponding to the various regions on the stress-strain curve can be rationalized:

1. During initial straining, dislocation slip in response to the applied stress resulted in strain hardening, which appeared to be the dominant deformation mechanism responsible for the positive slope on the stress-strain curve from the beginning to near the stress maximum. The replacement of the elongated recrystallized grains by smaller, equiaxed grains during straining is clearly a consequence of dislocation slip.
2. Early during SPF through the stress maximum, there was a small reduction in the population of the low angle subgrains accompanied by a corresponding increase in the population of the high angle grains. The process of their misorientation increase (to above 36°), however, was very rapid and abrupt, without a transition through the medium angle conditions, Figures 3(b) and 4(b). Within this strain range, there was no significant or abrupt increase in the (sub)grain size, Figure 2. Hence, the high angle grains could not have accumulated their misorientation by subgrain growth, subgrain coalescence or progressive grain rotation. These selected high angle grains must have undergone grain neighbor switching during GBS, in which low angle subgrains abruptly exchanged their low angle neighbors for high angle ones in a similar manner as described by Ashby and Verall [8].
3. From Figure 7(a), there was a gradual increase in the mean misorientation angle of the low angle subgrains, indicating grain rotation was steadily operative from the outset. Texture randomization due to grain rotation was not significant from the beginning to the stress maximum at $\varepsilon = 0.4$, as indicated by the peak intensity of the strong brass texture component remaining essentially unchanged within this strain range, Figure 9.
4. Once the subgrain mean misorientations reached past 7-8°, the fraction of high angle grains started to increase rapidly at the strain of about 0.4 corresponding to the stress maximum shown in Figure 1. This suggests a high rate of GBS at this point.
5. From $\varepsilon = 0.4$ to $\varepsilon = 0.75$, texture peak intensity dramatically dropped from 32 to 8 times random, suggesting that grain rotation was highly active. Accompanying this major texture randomization is the continued rapid increase in the fraction of high angle boundaries, Figure 7(b). This observation suggests that the combination of a higher fraction of high angle boundaries resulting from GBS along with the increase of the mean misorientation of subgrains to 7 or 8° provides the necessary conditions for easy grain rotation, which results in texture randomization.
6. Near $\varepsilon = 0.75$, most of the grains had become high angle in character. The optical grain structure showed features very similar to those at $\varepsilon = 1.3$, Figure 1. The corresponding ODF, Figure 9(f), also exhibited much diffuseness along with the loss of the brass texture to an intensity of 8 times random. The decreasing flow stress approached a plateau, Figure 1. Thus, the misorientation data, the optical structure, the microtexture and the flow stress all support the interpretation that the mode of deformation at this stage was dominated by extensive grain rotation, although GBS was expected to remain active.
7. The misorientation distribution at $\varepsilon = 1.3$, when compared to a simulated random grain structure with about 11,700 orientations [6], Figures 5(b, d), was indeed quite random. The initial brass texture was completely replaced by a nearly random texture, Figure 9(g), indicating continued random grain rotation. Thus, at $\varepsilon = 1.3$, the equiaxed grain structure was also associated with a nearly random texture.
8. Superimposed on this texture randomization process, however, an additional texture component appeared near the {110}<001> "Goss" position at $\varepsilon = 1.3$, Figure 9(g). This texture component was too weak to be identified in the conventional pole figure, but was quite apparent from the ODF analysis. Other investigators have also found situations of texture strengthening during SPF [9], although the specific texture components involved were different from the current study. The Goss texture is a known discontinuous recrystallization texture component, and has been previously found to be associated with the brass deformation texture [10]. Hence, the ODF analysis revealed that while the average microstructure evolved towards a random texture, a weak new texture component began to form at large strains. This effect, though small, adds another level of complexity to the underlying mechanisms of microstructure evolution during SPF.

Conclusion

1. No evidence of dynamic recrystallization was observed near the stress maximum at $\varepsilon = 0.4$, where a subgrain structure with a strong brass deformation texture still dominated.
2. Dislocation slip appeared to be responsible for the positive slope at the beginning portion of the stress-strain curve.
3. The abrupt increase of the misorientation of the low angle subgrains to high angle grains without a transition through the medium angle conditions indicated that GBS was operative early on before the stress maximum during SPF.
4. Grain rotation was operative steadily early on during SPF based on the progressive increase in the mean misorientation angle of the low angle subgrains with strain.
5. Grain rotation started to be very active at the stress maximum when the mean misorientation reached 7-8° and when the fraction of high angle grains was increasing rapidly.
6. The combination of a high fraction of high angle boundaries resulting from GBS and the higher mean misorientation of the low angle subgrain boundaries appear to be necessary conditions for easy grain rotation, which resulted in texture randomization.
7. At $\varepsilon = 0.75$, the mode of deformation was dominated by extensive grain rotation along with GBS.
8. At $\varepsilon = 1.3$, the equiaxed grain structure was associated with a nearly random texture.
9. A weak "Goss" texture, a known discontinuous recrystallization texture component, appeared at $\varepsilon = 1.3$.

Acknowledgments

The authors are grateful to the management of Alcoa for funding this work and for the permission to publish it. Stimulating discussions with Professor R. D. Doherty are greatly appreciated. Thanks are also due to Bob Burns for some of the misorientation measurements, Dale Ringer for the optical work and Dan Emmert for SPF tests.

References

1. B.M. Watts, M.J. Stowell, B.L. Baikie, and D.G.E. Owen, Metal Science 10, (1976), 189-197; ibid 10, (1976), 198-206.

2. S.J. Hales and T.R. McNelly, Acta Metall. 36, (1988), 1229-1239.

3. D.J. Chakrabarti, J.T. Staley, S.F. Baumann, R.R. Sawtell, P.E. Bretz and C.L. Jensen, US Patent No. 5,055,257, Oct. 8, 1991.

4. H. Gudmundsson, D. Brooks, and J.A. Wert, Acta Metall. 39, (1991), 19.

5. J. A. Venables and C. J. Harland, Phil. Mag. 27, (1973), 1193.

6. F. Barlat, Alcoa Internal Work.

7. H.J. Bunge, Texture Analysis in Materials Science, (London, Butterworths, 1982).

8. M.F. Ashby and R.A. Verall, Acta Metall. 21, (1973), 149-163.

9. R.H. Bricknell and J.W. Edington, Acta Metall. 27, (1979), 1303-1311.

10. J. Hjlen, R. Orsund, and E. Nes, Acta Metall. 39, (1991), 1377.